DC MicroGrids

Filipe Filipe.Perez@l2s.Centralesupelec.Fr Perez, Gilney Damm

Chapter 1

DC MicroGrids

Filipe Perez[1,2], **Gilney Damm**[3]

[1]L2S Laboratory, CentraleSupélec, Paris-Saclay University, Gif-Sur-Yvette, France
[2]Institute of Electrical Systems and Energy, Federal University of Itajubá, Itajubá, Brazil
[3]IBISC Laboratory, Paris-Saclay University, Evry, France

Abstract

This chapter introduces concepts of DC MicroGrids exposing their elements, features, modeling, control, and applications. Renewable energy sources, energy storage systems, and loads are the basics components of a DC MicroGrid. These components can be better integrated thanks to their DC feature, resulting in simpler power converter topologies, as well as the control strategy required for this application. A DC MicroGrid is developed as a realistic average model where the dynamics of the system are expressed in differential equations, including the nonlinearities of the model. A nonlinear distributed control strategy is developed for the DC MicroGrid, assuring the stability of the DC bus to guarantee the proper operation of each component of the MicroGrid. The energy storage systems are separated according to their time-scale operation, where a faster one (supercapacitor) controls voltage variations on the DC bus, and a slower one (battery) provides the power flow balance. The comparison with classical linear controllers is carried out to highlight the better performance of the nonlinear approach.

Keywords: DC MicroGrids, stability analysis, renewable source integration, energy storage systems, nonlinear control.

1.1 Introduction

The electrical grid is going through a revolution since the years 2000s. Such revolution is composed first by economic aspects as the liberalization of power markets and the unbundling and privatization of previously state-owned power companies. Next, because of environmental and social concerns, there has been a choice for reducing the use of fossil-based sources, and to some extent even nuclear power. This fundamental change of the power matrix has introduced ever-increasing shares of renewable energy sources (renewables). Such changes, if continued in the future, will completely reshape the way power grids operate, in particular because the two previous points (economic and environmental) are rather antagonistic. Also, renewables introduce large variability in the electrical grid, which need a perfect equilibrium at all time on the produced and consumed electric power. The solution to attain stability in such time-varying production and consumption has been the introduction of new elements from Information and Communication Technologies (ICT). Such merge of traditional power grids with ICT is now known as *SmartGrids* [1, 2, 3].

SmartGrids are composed of several elements, among them the concept of *MicroGrids*. MicroGrids are small portions of the electric grid that can to some extent balance itself with the production and consumption of electricity and can stabilize its fundamental states. In the case where the MicroGrid is always connected to the main grid, thus importing and exporting arbitrary amounts of power, the MicroGrid is said to be in grid-connected mode. In this case, the MicroGrid is kept synchronized to the main grid, and as a consequence, frequency, angle, and inertia phenomena are dealt with by the main grid. In this case, the MicroGrid only needs to assure voltage stability and mitigation of power congestion in lines, and maximize some power consumption pattern. This maximization may be regarding auto-consumption, renewables' share, profit, among others, and will be obtained by managing its production, the amount of power imported from the main grid, and possibly the use of storage [4, 5, 6].

In the case where the MicroGrid may be disconnected (or at least not be synchronized) from the main grid, the MicroGrid is said to be in island mode. In this case, the MicroGrid is responsible for keeping stability in all states that compose it, i.e., frequency, angle (mainly inertia problems), voltage, power flux congestion, and profit. This case is far more complicated than the first. Then, if there is at least one large synchronous generator in the MicroGrid, a diesel generator for example, that provides the largest share of the consumed power, then the system degenerates to the standard isolated MicroGrids one can find in remote locations. But when larger shares of renewables are present in such grids, the problem may become very complex [6, 7, 8].

Renewables have some characteristics that completely distinguish them from other power sources. The most important is the fact that renewables are not controlled. Wind, sun, tides, and other natural phenomena are uncorrelated with the needs of consumers. For this reason, it is not possible to have at all time the production that matches the consumption; this intermittent production is the largest challenge renewables pose, and must be considered either in the

framework of power and of energy. A second characteristic is that most renewables have large dispersion. For this reason, electric production by renewables is often distributed, and then much harder to be integrated. Thus, renewables are mostly integrated into the low and medium voltage levels, which is in complete antagonism with the way power systems were designed [9, 10, 11].

Another important aspect is the significant number of people in remote communities living without access to electricity. These villages may never have grid connection because of economic reasons and remoteness. On the other hand, many of isolated communities, such as African, Brazilian, or island communities, have great potential for solar radiation and wind, allowing for the use of renewables. Electricity supply can be seen as a contribution to social inclusion and improvement of the quality of life where electricity is mainly used for household purposes such as lighting, heating, and others to meet local energy demand [12, 13]. In addition, the transition for an electricity based energy usage avoids consuming local carbon-based resources like coal or wood. This helps to improve the conservation of ecosystems and mitigation of CO_2 emissions.

The stand-alone grid application (island mode) requires a proper operation to provide reliable, continuous, sustainable, and good-quality electricity to consumers, which brings several technical challenges for renewables application. The intermittent and non-dispatchable characteristic of renewables cause great impacts related to instability and fluctuations in their energy generation. In this context, the use of energy storage systems coupled with renewables operating to supply a local load properly has brought the MicroGrid concept, which is a powerful solution to accomplish the targets of stand-alone grid operation, improving reliability, resilience, and availability of the whole system [3, 14, 15].

MicroGrids may indeed bring an important answer for most of these problems and may represent in the future the new standard for power systems. Nevertheless, it is still a very difficult problem, and much effort is necessary to make such grids a widespread reality.

In the MicroGrid context, direct current (DC) MicroGrids are seen as a major advantage, since renewables (PV, Wind, fuel cells), electronic loads, electric vehicles, and storage (batteries, supercapacitors) have DC nature. If they are connected through a DC grid, they would need a smaller number of converters, and those converters would be simpler than if they are connected through an AC grid. The result would be less expensive materials, and better efficiency (fewer losses). Also, direct current can be more efficient due to its simpler topology; the absence of reactive power and frequency to be controlled; the harmonic distortion is not a problem anymore; and there is no need of synchronization with the network. The consequence is a simpler control structure based on the interaction of currents between the converters, being the DC bus voltage the main control priority, that is, the voltage is a natural indicator of power balance conditions. At the same time, the DC MicroGrid is a challenge because the structure of the current power grid, power supplies, transformers, cables, and protection is designed in alternating current. For this reason, hybrid AC/DC MicroGrid is seen as a compromise between AC and DC to allow for better integration of these new devices and the classical electric grid [16, 17, 18]. Figure

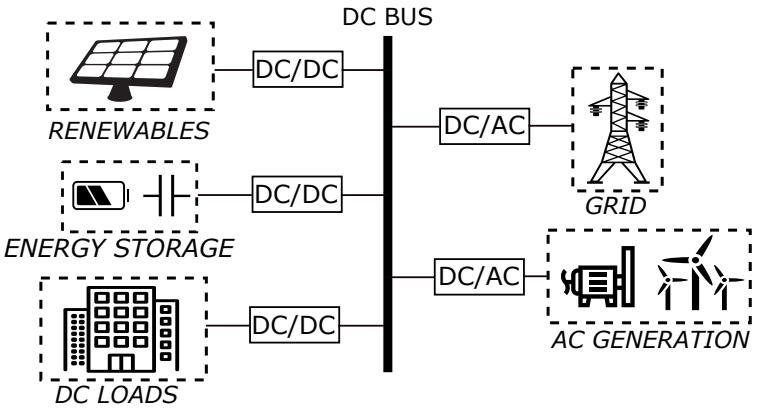

Figure 1.1: A general DC MicroGrid scheme.

1.1 depicts a general DC MicroGrid composed of renewables generation, energy storage system, loads and grid-connection.

Nowadays there exist several examples of small DC MicroGrids, as in marine, aviation, automotive, and manufacturing industries. In all these examples it is extremely important that the MicroGrid is controlled such a way to present reliability and proper operation. To attain this goal, there are many control strategies proposed for MicroGrids. The linear technique is the most popular one, due its simplicity and robustness; in addition linear control is well known for both academia and industry. Linear control is based on a linearized model given by the electrical circuit equations of the MicroGrid, where the nonlinearities are not considered. As a consequence, this simplified model is only valid in a small region around the operation point where the linearization was made. There are several approaches for linear control, for example in frequency domain via transfer functions or by space state modeling, which is a time domain manner to represent the system' dynamics, where PID, state feedback and LQR allocation of poles are viable strategies. The minor loop gain is another example of linear technique that relates source and load impedances to determine stability in the grid, this strategy maintains the system dynamics even connecting more devices like filters. The impedance-based approach provides a good perspective on dynamics like the well-known state space modeling [15, 19, 20].

Nonlinear control on the other hand is based on a complete model of the system, in the sense that nonlinear dynamics and the whole operation space are considered. Then, the nonlinear theory allows for a more realistic grid modeling, a more effective stability analysis, and a broader range of operation. The utilization of nonlinear control techniques may also improve power flow performances in the MicroGrid, since the system is not restricted by an operating point, and there is the possibility to work in a wider region of operation, considering just the physical limitations of the system as restrictions. A drawback of the use of nonlinear control technique is the increased complexity of analysis

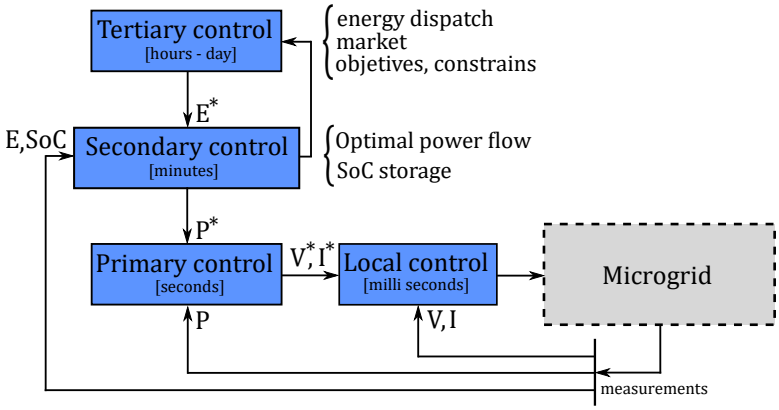

Figure 1.2: The traditional hierarchical control structure for a DC MicroGrid. The local and primary control generate the references for lower level power converters, while the secondary control deals with power flow regulation and the tertiary control covers the energy dispatch and energy market

and sometimes in the resulting control law, which is sometimes harder to be implemented [21, 22, 23, 24].

1.1.1 Hierarchical Structure

To provide proper operation of the system, it is necessary to implement a full control strategy involving different time scales, referring to a hierarchical control structure. The hierarchical control structure spans local, primary, secondary, and tertiary controllers, ranging from milliseconds to hours or a day. Figure 1.2 describes the hierarchical structure in a DC MicroGrid.

The local controllers are the mathematical algorithms that assure stability of the lower level variables and counteract disturbances with fast response, good transient and steady-state performances. The local controllers then ensure the transient stability of the system in milliseconds to seconds, and currents and voltages references are given by higher level controllers. The local control acts on the power converters of the MicroGrid devices using their PWM modulation to control the converters' dynamics [25, 26].

The primary control operates in a time range of a few seconds; its responsibility is to adapt the grid operation points to a disturbance acting during the time interval the secondary controller needs to calculate new optimal operation set points. For smaller MicroGrids, the primary can be integrated into the local controller, in a master–slave approach. In this case, one converter is assumed to keep the grid's stability (master).

The secondary level controller carries out the power flow regulation of the system taking into account the state-of-charge (SoC) of energy storage systems (battery and supercapacitor), then an optimal power flow is generated. The

power flow is calculated by sharing the load demand in the system among the renewables generation and the storage elements also taking care of their SoC to allow for proper functioning and save battery lifetime. The secondary control provides a reference of power to the grid assuring power balance in the system. The secondary is also related to power quality requirements and device operating limits where the constraints must be respected [27, 28].

The tertiary control deals with the energy market, organizing the energy dispatch schedule according to an economic point of view, taking into account negotiation between consumers and producers. This level also deals with human–machine interaction and social aspects [29, 25].

1.2 MicroGrid Modeling

A usual DC MicroGrid is composed by a variable load, an energy source (e.g., a PV array), and an energy storage system (a battery, a supercapacitor among others, or a hybrid application of them).

Figure 1.3 introduces the considered DC MicroGrid, which is composed by a supercapacitor, a battery, a PV array, and a variable load (e.g., household appliances or an electric vehicle). Each device is connected to a DC bus by a DC/DC converter: they are bidirectional-boost for supercapacitor and battery, a boost for PV and a buck for the load.

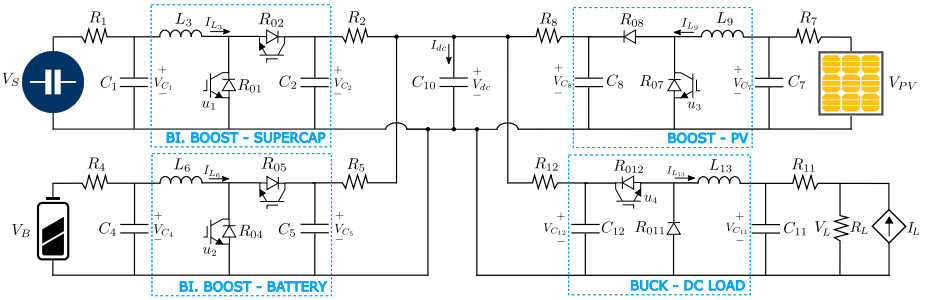

Figure 1.3: The DC MicroGrid integrating the PV array as main power generation and the two energy storage systems operating at different time scales to feed a local DC load

At this point, it is important to distinguish the effects of power and energy in the MicroGrid. The dynamic of the average voltage of a MicroGrid is modeled by Eq. (1.14) based on capacitor C_{10} shown in Figure 1.3. This voltage varies instantaneously as a function of the balance of instantaneous **power** fed in or consumed in the grid. To keep this voltage stable, it is necessary to provide or absorb a suitable amount of power driven by a control law. The variations of power will be as fast as loads/sources vary, and as fast as the control law was designed to be. These variations will imply in current variations from the storage elements. Even though a battery could in many cases provide the

necessary power variation, such behavior severely reduces its lifetime. For this reason, it is preferable to use a supercapacitor (or flywheel) to perform this task. On the other hand, a supercapacitor even if can provide large power bursts, has a rather small energy stored. For this reason, it is necessary to couple it with a larger storage unit like a battery to provide the necessary energy balance in a certain operation time. The battery (or another slower storage) will then assure the long-term energy balance, while the supercapacitor (or other fast storage) assures the instantaneous power balance.

The microgrid control target is to properly operate each device of the system and keep the stability of the whole system at the same time. Therefore, the following objectives must be fulfilled: the PV array is controlled to work at the maximum power point; the battery is controlled to perform the balance on the power flow with slow speed dynamics; the supercapacitor stabilizes the DC bus such that the DC load is properly supplied. Two assumptions are necessary here: a higher level controller is supposed to provide references to be accomplished by the local controllers [5]; there is proper sizing of PV array, battery, and supercapacitor to have a feasible power balance concerning the sizing of the load [21].

The local controllers are responsible to control each physical device of this MicroGrid. The primary control must be able to generate the appropriate reference signals for the local controllers, and has to follow the references provided by the secondary. The task of secondary control will be to schedule power transfer between the network nodes providing voltage and power references to local and primary controllers. In order to carry out this task, communication between nodes and secondary controller must exist. The references for lower controllers will be the result of periodic power flows. Desired power flow indications come from the tertiary controller, in order to attain optimality for some objective. In general, the objective is a mix of economic profit, maximization of local production (minimization of imports) and minimization of CO_2 emissions. The main variables in this level are related to price, energy, and human factors such as comfort.

1.2.1 Supercapacitor System

The supercapacitor is an energy storage applied in power systems to improve power quality, due its fast response to grid oscillations. The supercapacitor can offer higher power density and increased life cycles but still has a considerably lower energy density. Then it can be combined with the battery characteristics, such that the capacitor can act in the grid transients and the battery may deal with the power flow [30]. We can consider a supercapacitor to provide voltage stability in the studied MicroGrid system. In this case, a bidirectional-boost converter connects the supercapacitor in the DC link. The average state-space model is presented in (1.1)-(1.3):

$$\dot{V}_{C_1} = \frac{1}{R_1 C_1} V_S - \frac{1}{R_1 C_1} V_{C_1} - \frac{1}{C_1} I_{L_3} \tag{1.1}$$

$$\dot{V}_{C_2} = \frac{1}{R_2 C_2} V_{dc} - \frac{1}{R_2 C_2} V_{C_2} + \frac{1}{C_2} I_{L_3}(1 - u_1) \tag{1.2}$$

$$\dot{I}_{L_3} = \frac{1}{L_3} V_{C_1} - \frac{1}{L_3} V_{C_2}(1 - u_1) - \frac{R_{01}}{L_3} I_{L_3} \tag{1.3}$$

V_S is the supercapacitor's voltage, V_{C_1} is the voltage on capacitor C_1, V_{C_2} is the voltage on capacitor C_2, I_{L_3} is the current on inductor L_3. R_1 and R_2 are the resistances representing the cable losses, R_{01} and R_{02} represent switch losses of the semiconductors and u_1 is the duty cycle of the converter. For bidirectional converters we can consider $R_{01} = R_{02}$.

1.2.2 Battery System

The battery bank may be a lithium-ion one for example, which has a higher energy density, longer life cycle and absence of memory effect compared with other storagebattery technologies [9, 31]. The target of the battery can be to regulate the power flow in the system according to the secondary level control, then this system has to be properly sized to inject or absorb the right amount of power. The battery has a piecewise constant power supply, which is a smooth way that maximizes its lifetime. A bidirectional-boost converter is used to integrate the battery in the MicroGrid. The average state-space model of the battery converter is written in (1.4)-(1.6):

$$\dot{V}_{C_4} = \frac{1}{R_4 C_4} V_B - \frac{1}{R_4 C_4} V_{C_4} - \frac{1}{C_4} I_{L_6} \tag{1.4}$$

$$\dot{V}_{C_5} = \frac{1}{R_5 C_5} V_{dc} - \frac{1}{R_5 C_5} V_{C_5} + \frac{1}{C_5} I_{L_6}(1 - u_2) \tag{1.5}$$

$$\dot{I}_{L_6} = \frac{1}{L_6} V_{C_4} - \frac{1}{L_6} V_{C_5}(1 - u_2) - \frac{R_{04}}{L_6} I_{L_6} \tag{1.6}$$

V_B is the battery's voltage, V_{C_4} is the voltage on capacitor C_4, V_{C_5} is the voltage on capacitor C_5, I_{L_6} is the current on inductor L_6. R_4 and R_5 are the resistances representing the cable losses, R_{04} and R_{05} are switch losses of the semiconductors and u_2 is the duty cycle of the converter. In this case, we can also consider $R_{04} = R_{05}$

1.2.3 PV System

The PV array is often the main generation in the MicroGrid since it is a well-known renewable source, widely applied in industrial, commercial or residential buildings. At the same time, there are many subsidies and social concern with environment preservation for renewables integration. A MPPT (Maximum

Power Point Tracking) algorithm is necessary to always extract the maximum energy of the PV according to the variation of sun irradiance. There are many algorithms in literature, the most famous are Perturbation and Observation (P&O) and incremental conductance because their fast response and simplicity [32, 33]. The DC/DC converter controls the PV according to the MPPT reference to optimize the power generation in the MicroGrid. A boost converter is used to connect the PV into DC bus and the state-space model of the PV converter can be written in (1.7)-(1.9).

$$\dot{V}_{C_7} = \frac{1}{R_7 C_7} V_{PV} - \frac{1}{R_7 C_7} V_{C_7} - \frac{1}{C_7} I_{L_9} \tag{1.7}$$

$$\dot{V}_{C_8} = \frac{1}{R_8 C_8} V_{dc} - \frac{1}{R_8 C_8} V_{C_8} + \frac{1}{C_8} I_{L_9}(1 - u_3) \tag{1.8}$$

$$\dot{I}_{L_9} = \frac{1}{L_9} V_{C_7} - \frac{1}{L_9} V_{C_8}(1 - u_3) - \frac{R_{08}}{L_9} I_{L_9} + \frac{1}{L_9}(R_{08} - R_{07}) I_{L_9} u_3 \tag{1.9}$$

V_{pv} is the panel's voltage, V_{C_7} is the voltage on capacitor C_7, V_{C_8} is the voltage on capacitor C_8, I_{L_9} is the current on inductor L_9. R_7 and R_8 are the resistances representing the cable losses, R_{07} and R_{08} are switch losses of the semiconductors and u_3 is the duty cycle of the converter.

1.2.4 DC Load System

The DC load in the MicroGrid can be generalized to represent lights, ventilation, heating and even an electrical vehicle. Therefore, the load can be considered as time varying dynamic, shifting the power according to the required demand [10]. The load voltage is usually set in a constant value and must be maintained inside the grid constraints (in general $\pm 5\%$ of nominal value), given by the regulatory standards. A buck converter integrates the DC load into the grid. The state-space model of the load converter can be written in (1.10)-(1.12).

$$\dot{V}_{C_{11}} = \frac{1}{R_{11} C_{11}} V_L - \frac{1}{R_{11} C_{11}} V_{C_{11}} + \frac{1}{C_{11}} I_{L_{13}} \tag{1.10}$$

$$\dot{V}_{C_{12}} = \frac{1}{R_{12} C_{12}}(V_{dc} - V_{C_{12}}) - \frac{1}{C_{12}} I_{L_{13}} u_4 \tag{1.11}$$

$$\dot{I}_{L_{13}} = -\frac{1}{L_{13}} V_{C_{11}} - \frac{R_{011}}{L_{13}} I_{L_{13}} + \frac{1}{L_{13}}\left[V_{C_{12}} - (R_{012} - R_{011}) I_{L_{13}}\right] u_4 \tag{1.12}$$

V_L is the load voltage, $V_{C_{11}}$ is the voltage on capacitor C_{11}, $V_{C_{12}}$ is the voltage on capacitor C_{12}, $I_{L_{13}}$ is the current on inductor L_{13}. R_{11} and R_{12} are the resistances representing the cable losses, R_{011} and R_{012} are switch losses of the semiconductors and u_4 is the duty cycle of the converter.

The load can be represented as a variable current source I_L with a fixed resistance in parallel R_L. Then, the variation in the current source I_L represent

the load demand variation, directly related by the load impedance as follows.

$$I_L = \frac{1}{R_{11}}(V_{C_{11}} - V_L) - \frac{V_L}{R_L}$$

The load model as a current source brings simplicity for the simulation structure.

1.2.5 MicroGrid DC bus

The DC bus is the common coupling point of all devices in the MicroGrid. If we take a look in the node on DC capacitor C_{10}, it is possible analyze all currents flowing into the system. The node in the DC bus can be described as follows:

$$I_{dc} = I_{R_2} + I_{R_5} + I_{R_8} + I_{R_{12}} \tag{1.13}$$

Rewriting (1.13) using the known parameters, the DC bus dynamic is represented in (1.14).

$$\dot{V}_{dc} = \frac{1}{C_{10}}\left[\frac{1}{R_2}(V_{C_2} - V_{dc}) + \frac{1}{R_5}(V_{C_5} - V_{dc}) + \right. \\ \left. + \frac{1}{R_8}(V_{C_8} - V_{dc}) + \frac{1}{R_{12}}(V_{C_{12}} - V_{dc})\right] \tag{1.14}$$

The voltage's dynamic in the DC bus can be seen as the sum of currents in each device of the MicroGrid, then the stability of the DC bus need to take into account each element connected in this DC bus, resulting in complex stability analysis. The supercapacitor system is chosen to control the DC bus; then supercapacitor will absorb/inject power according to voltage imbalance on DC bus. Now, with all system dynamics modeled, it is possible to develop the control strategies of the MicroGrid.

1.3 Control Strategy

This section describes the control strategy of each system and the stabilization analysis of the whole grid.

A "plug-and-play" approach based on the "system of systems" philosophy using distributed control methodologies is developed for DC MicroGrid since it can work better in isolated systems. Therefore, the supercapacitor is designed to regulate the voltage V_{dc} by controlling the output voltage V_{C_2} on its converter, which regulates the fast oscillations and transients of the DC bus. The reference for the battery is the current $I^*_{L_6}$, which is given by the second level controller to control the slower variations on the grid and the state of charge of the supercapacitor. The reference for the PV is current I_{L_9} calculated by the MPPT algorithm to extract the maximum power from the PV array. Finally, the control target in the DC load is to maintain voltage $V_{C_{11}}$ on the desired constant value $V^*_{C_{11}}$.

1.3.1 Feedback Linearization for Supercapacitor

The supercapacitor control target is to regulate the DC bus voltage V_{dc} to assure the stability of its dynamic. For this, the voltage V_{C_2} is the control input chosen to accomplish this target. Therefore, we can control V_{dc} by driving V_{C_2} to the desired voltage $V_{C_2}^*$, such that, V_{dc} is stabilized.

The control structure follows the consideration: the supercapacitor system (1.1)-(1.3) is composed of two subsystems, first the current subsystem (I_{L_3}) and second the voltages' subsystem (V_{C_1},V_{C_2} and V_{dc}). There is a control law, such that the current subsystem is designed to display much faster dynamics than the voltages' subsystem. Therefore, by properly choosing the convergence speed of both subsystems we create the singular perturbation condition based on explicit time-scale separation (see [34]).

Since I_{L_3} will be controlled to have much faster dynamics than the voltages, under some mild conditions the controllers can be developed separately [35]. First, we propose the control design to steer $I_{L_3} \to I_{L_3}^*$, where $I_{L_3}^*$ is yet to be designed. Thus, $I_{L_3}^*$ will be deduced based on a simplified model for V_{C_2} obtained by singular perturbation. The control $I_{L_3}^*$ is designed such as to steer V_{C_2} to $V_{C_2}^*$, where $V_{C_2}^*$ is designed such as to stabilize the DC link in the MicroGrid.

Current subsystem control law

The first step is to control the current I_{L_3} to its reference $I_{L_3}^*$. According to the control objective, let us define the output as $y_1 = I_{L_3}$. It is considered that the system has one output and one input, thus a square system as shown in (1.15).

$$\begin{cases} \dot{I}_{L_3} = f_1(V_{C_1}, V_{C_2}, I_{L_3}) + g_1 u_1 \\ y_1 = I_{L_3} \end{cases} \tag{1.15}$$

The Lie derivative of the output with respect to g_1 is:

$$J_1 = -\frac{V_{C_2}}{L_3}$$

J_1 is non-singular since V_{C_2} is always positive by technological reasons, therefore a nonlinear feedback linearizing control input can be written as:

$$\begin{aligned} u_1 &= J_1^{-1}\left[v_3 - \frac{1}{L_3}\left(V_{C_1} - V_{C_2} - R_{01} I_{L_3}\right)\right] \\ &= 1 + \frac{1}{V_{C_2}}\left[L_3 v_3 - V_{C_1} + R_{01} I_{L_3}\right] \end{aligned}$$

where v_3 is the additional input to be designed.

Since $I_{L_3}^*$ is the desired trajectory for I_{L_3}, it is possible to design the additional input v_3 in a linear manner with respect to the output I_{L_3} and hence a linear stable subspace is generated.

$$\begin{aligned} v_3 &= \dot{I}_{L_3}^* - K_3(I_{L_3} - I_{L_3}^*) - K_3^{\alpha}\alpha_3 \\ \dot{\alpha}_3 &= I_{L_3} - I_{L_3}^* \end{aligned}$$

where K_3 and K_3^{α} are positive constants.

v_3 is the desired dynamics of I_{L_3} and α_3 an auxiliary variable. This can be interpreted as a pole placement from linear control theory.

Voltages' subsystem control law

Now, the crucial step is to properly calculate the reference value $I_{L_3}^*$, such that $V_{C_2} \to V_{C_2}^*$. Here, the task is to design a slowly varying $I_{L_3}^*$ whose derivative has minimum effect in the current control designed previously.

From singular perturbation analysis, we can consider that I_{L_3} has already reached $I_{L_3}^*$ on V_{C_2} dynamics because of time-scale separation (I_{L_3} is considered much faster than V_{C_2}). Therefore, we may replace V_{C_2} dynamics as follows [36, 37, 38, 39].

$$\dot{V}_{C_2} = \frac{1}{R_2 C_2} V_{dc} - \frac{1}{R_2 C_2} V_{C_2} + \frac{1}{C_2} I_{L_3}^* (1 - u_1^*) \tag{1.16}$$

where:

$$u_1^* = 1 - \frac{1}{V_{C_2}} [V_{C_1} - R_{01} I_{L_3}^*]$$

that result as:

$$\dot{V}_{C_2} = \frac{1}{R_2 C_2} (V_{dc} - V_{C_2}) + \frac{I_{L_3}^*}{C_2 V_{C_2}} [V_{C_1} - R_{01} I_{L_3}^*] \tag{1.17}$$

Using singular perturbation we have obtained this simplified model of V_{C_2}, then as a next step, one may choose $v_d = \dot{I}_{L_3}^*$, which represents a dynamical feedback approach. With v_d as the new control input, there is a full state transformation with no zero dynamics. Besides that, we can find the control reference $I_{L_3}^*$ by integrating the new control input $I_{L_3}^* = \int v_d dt$.

Applying input/output feedback linearization theory and defining V_{C_2} as the control output, the relative degree is 2. Consequently, we may find v_d in the second time-derivative of the simplified V_{C_2} dynamics. The following Lie derivatives can be deduced as:

$$\dot{V}_{C_2} = L_{f_2}^1 h_2(x) \tag{1.18}$$

$$\ddot{V}_{C_2} = \frac{\dot{V}_{dc}}{R_2 C_2} - \dot{V}_{C_2} \left[\frac{1}{R_2 C_2} + \frac{V_{C_1} I_{L_3}^* - R_{01} {I_{L_3}^*}^2}{C_2 {V_{C_2}}^2} \right] + \frac{1}{C_2 V_{C_2}} I_{L_3}^* \dot{V}_{C_1} + \frac{1}{C_2 V_{C_2}} (V_{C_1} - 2 R_{01} I_{L_3}^*) \dot{I}_{L_3}^* \tag{1.19}$$

Therefore, we have found the control input v_d as:

$$\ddot{V}_{C_2} = L_{f_2}^2 h_2(x) + L_{g_2} L_{f_2}^1 h_2(x) v_d \tag{1.20}$$

By introducing a synthetic input θ_d, the input v_d can be designed as:

$$v_d = \frac{1}{L_{g_2} L_{f_2}^1 h_2(x)} [\theta_d - L_{f_2}^2 h_2(x)] \tag{1.21}$$

where the additional input is chosen using linear techniques to assign the desired dynamics for V_{C_2}.

$$\theta_d = -K_2(\dot{V}_{C_2} - \dot{V}_{C_2}^*) + K_2^\alpha (V_{C_2} - V_{C_2}^*) \tag{1.22}$$

By substituting (1.21) and (1.22) in (1.17) and (1.20), the following closed-loop is obtained:

$$\begin{bmatrix} \dot{V}_{C_2} \\ \ddot{V}_{C_2} \end{bmatrix} = \begin{bmatrix} 0 & 1 \\ -K_2^\alpha & -K_2 \end{bmatrix} \begin{bmatrix} V_{C_2} - V_{C_2}^* \\ \dot{V}_{C_2} - \dot{V}_{C_2}^* \end{bmatrix}$$

where we can define the speed of convergence for V_{C_2}, using K_2 and K_2^α by pole placement to get slower voltage dynamics for the simplified model.

Remark 1: One of the tasks is to design a slowly varying $I_{L_3}^*$ whose derivative has negligible effects on the current subsystem.

Remark 2: The use of singular perturbation to obtain the simplified model is valid inside an operating region that is given by the time scale ratio from the two subsystems. As a consequence, the desired imposed dynamics should be chosen such as to obtain a suitable operation region for the DC MicroGrid (see [34]).

Remark 3: In the proposed control law, the dynamical feedback linearization approach was applied in order to obtain a full state transformation, resulting in a linear second-order system.

1.3.2 DC grid stabilization

The DC bus voltage must be controlled to assure proper operation of each device of the DC MicroGrid. Then, the stability of V_{dc} is extremely important for the system operation. The voltage V_{dc} should be kept at a constant value V_{dc}^*, therefore voltage V_{C_2} is controlled such that $V_{dc} \to V_{dc}^*$.

In this case, the output voltages of the power converters of the MicroGrid compose the DC bus dynamics, and the stability analysis of these variables are needed to be studied. For this, we may propose a complete Lyapunov function composed of all dynamics of the DC bus. The Lyapunov function candidate is written in (1.23), where $V_{C_5}^e$, $V_{C_8}^e$ and $V_{C_{12}}^e$ are the equilibrium points of V_{C_5}, V_{C_8} and $V_{C_{12}}$ respectively.

$$W(x) = \frac{C_{10}}{2} V_{dc}^2 + \frac{C_5}{2}(V_{C_5} - V_{C_5}^e)^2 + \frac{C_8}{2}(V_{C_8} - V_{C_8}^e)^2 + \tag{1.23}$$
$$+ \frac{C_{12}}{2}(V_{C_{12}} - V_{C_{12}}^e)^2 + \frac{C_{15}}{2}(V_{C_{15}} - V_{C_{15}}^e)^2 + \frac{C_{17}}{2}(V_{C_{17}} - V_{C_{17}}^e)^2$$

Now, to investigate the stability of the DC bus, we may compute the time derivative of $W(x)$. In order to obtain a simpler algorithm, we assign the dynamics of V_{dc} to be much slower than V_{C_2} by setting constant K_2 from (1.22)

much bigger than $\frac{1}{C_{10}R_2}$ in (1.14) (which means $K_2 >> \frac{1}{C_{10}R_2}$) . Resulting again in a explicit time-scale separation, then from singular perturbation analysis, V_{C_2} is considered as having already reached its equilibrium point $V^*_{C_2}$. In fact, we have three subsystems in different time scales, with current I_{L_3} being the fastest one, V_{C_2} in the middle and V_{dc} the slowest one.

$$\dot{W}(x) = V_{dc}\Bigg[\frac{1}{R_2}(V^*_{C_2} - V_{dc}) + \frac{1}{R_5}(V_{C_5} - V_{dc}) + \frac{1}{R_8}(V_{C_8} - V_{dc}) + \tag{1.24}$$
$$+\frac{1}{R_{12}}(V_{C_{12}} - V_{dc})\Bigg] + (V_{C_5} - V^e_{C_5})\Bigg[\frac{1}{R_5}(V_{dc} - V_{C_5}) + I_{L_6}(1-u_2)\Bigg] +$$
$$+(V_{C_8} - V^e_{C_8})\Bigg[\frac{1}{R_8}(V_{dc} - V_{C_8}) + I_{L_9}(1-u_3)\Bigg] +$$
$$+(V_{C_{12}} - V^e_{C_{12}})\Bigg[\frac{1}{R_{12}}(V_{dc} - V_{C_{12}}) - I_{L_{13}}u_4\Bigg]$$

To obtain a stable grid connection, we analyze the time derivative of $W(x)$ where the desired expression for $\dot{W}(x)$ is presented as follows:

$$\dot{W}(x) = -\frac{1}{R_2}(V^2_{dc} - V^{*\,2}_{dc}) - \frac{1}{R_5}(V_{C_5} - V^e_{C_5})^2 + \tag{1.25}$$
$$-\frac{1}{R_8}(V_{C_8} - V^e_{C_8})^2 - \frac{1}{R_{12}}V_{C_{12}} - V^e_{C_{12}})^2$$

The Lyapunov function (1.23) then results to be an ISS-like Lyapunov function with equilibrium point in V^*_{dc} [40, 41]. Here, $V^*_{C_2}$ is the control input that can regulate V_{dc} in the desired value and assure asymptotic stability for those dynamics. Therefore, the following control input is assigned to be the desired $V^*_{C_2}$, such that one obtains (1.25) as the time-derivative of $W(x)$.

$$V^*_{C_2} = \frac{R_2}{V_{dc}}\Bigg\{\frac{1}{R_2}V^*_{dc} - V_{dc}\Bigg[\frac{1}{R_5}(V_{C_5} - V_{dc}) + \frac{1}{R_8}(V_{C_8} - V_{dc}) + \tag{1.26}$$
$$+\frac{1}{R_{12}}(V_{C_{12}} - V_{dc})\Bigg] - (V_{C_5} - V^e_{C_5})\Bigg[\frac{1}{R_5}(V_{dc} - V^e_{C_5}) + I_{L_6}(1-u_2)\Bigg] +$$
$$-(V_{C_8} - V^e_{C_8})\Bigg[\frac{1}{R_8}(V_{dc} - V^e_{C_8}) + I_{L_9}(1-u_3)\Bigg] +$$
$$-(V_{C_{12}} - V^e_{C_{12}})\Bigg[\frac{1}{R_{12}}(V_{dc} - V^e_{C_{12}}) - I_{L_{13}}u_4\Bigg]\Bigg\}$$

With the above conditions we obtain an asymptotically stable equilibrium point [42], provided that V_{C_2} is stabilized to $V^*_{C_2}$, and then one can assure voltage regulation for the DC voltage bus.

Remark: In the procedure above, we have used twice the singular perturbation theory such as to obtain (even if restricted to an operation region) much simpler controllers based on simplified models. In this way, the derivatives of $\dot{V}_{dc}$ and $\dot{V}_{C_2}$ can be neglected.

Such successive derivatives may be hard to compute and in general, have a very small contribution to the control. This can be understood either mathematically as a result of relative very slow dynamics compared to the previous, or technologically as the contribution of small capacitors compared to the remaining dynamics from the converters. From the theoretical point of view the speed of convergence for V_{dc} ($K_{10} = 1/R_2$ from (1.25)) is assigned to be much slower than the voltage V_{C_2} (given by K_2 and K_2^α). Therefore, the time-scale separation provides that $\dot{V}_{C_2}^*$ can be neglected on equation (1.22).

1.3.3 Feedback linearization for battery

The reference $I_{L_6}^*$ for the battery's converter is provided by the secondary controller, based on the power flow regulation and state of charge of the supercapacitor. The battery is responsible for supplying the power imbalance between PV generation and load demand, taking into account its SoC level and acting with piecewise constant variations to save its lifetime. This can be a complex target for secondary control, and therefore the supercapacitor can assume the target to respond in fast variation not considered for the battery. According to the control objective, let us define the considered output as $y_2 = I_{L_6}$. It is considered that the system has one output and one input, and thus a square system is shown in (1.27).

$$\begin{cases} \dot{I}_{L_6} = f_2(V_{C_4}, V_{C_5}, I_{L_6}) + g_2 u_2 \\ y_2 = I_{L_6} \end{cases} \tag{1.27}$$

The Lie derivative of the output with respect to g_2 is:

$$J_2 = -\frac{V_{C_5}}{L_6}$$

J_2 is non-singular since V_{C_5} is always positive by technological reasons, and therefore a nonlinear feedback linearizing control input can be written as:

$$\begin{aligned} u_2 &= J_2^{-1}\left[v_6 - \frac{1}{L_6}\left(V_{C_4} - V_{C_5} - R_{04} I_{L_6}\right)\right] \\ &= 1 + \frac{1}{V_{C_5}}\left[L_6 v_6 - V_{C_4} + R_{04} I_{L_6}\right] \end{aligned}$$

where u_2 is the control input in (1.27) and v_6 is the additional input.

Since $I_{L_6}^*$ is the desired trajectory for I_{L_6}, it is possible to design the additional input v_6 in a linear manner with respect to the output I_{L_6} and hence a linear stable subspace is generated.

$$\begin{aligned} v_6 &= \dot{I}_{L_6}^* - K_6(I_{L_6} - I_{L_6}^*) - K_6^\alpha \alpha_6 \\ \dot{\alpha_6} &= I_{L_6} - I_{L_6}^* \end{aligned}$$

where K_6 and K_6^α are positive constants.

Zero dynamics

The states V_{C_4} and V_{C_5} are the zero dynamics in the battery system. The calculated equilibrium points are given by:

$$V_{C_4}^e = V_B - R_4 I_{L_6}^*$$

$$V_{C_5}^e = \frac{V_{dc}}{2} \pm \frac{1}{2}\sqrt{V_{dc}^2 + 4R_5 I_{L_6}^*(V_{C_4} - R_{04} I_{L_6}^*)}$$

To analyze the zero dynamics stability, the Jacobian linearization matrix B is presented bellow:

$$B = \begin{bmatrix} -\frac{1}{R_4 C_4} & 0 \\ \frac{1}{C_5}\frac{I_{L_6}^*}{V_{C_5}} & -\frac{1}{R_5 C_5} - \frac{I_{L_6}^*(V_{C_4} - R_{04} I_{L_6}^*)}{C_5 {V_{C_5}^e}^2} \end{bmatrix}$$

The eigenvalues of λ can be written as:

$$\lambda_{1,2} = -\frac{c}{2} \pm \frac{1}{2}\sqrt{c^2 - 4d}$$

where:

$$c = \frac{1}{R_4 C_4} + \frac{1}{R_5 C_5} + \frac{I_{L_6}^*}{C_5 {V_{C_5}^e}^2}(V_{C_4} - R_{04} I_{L_6}^*) \tag{1.28}$$

$$d = \frac{1}{R_4 C_4}\left[\frac{1}{R_5 C_5} + \frac{I_{L_6}^*}{C_5 {V_{C_5}^e}^2}(V_{C_4} - R_{04} I_{L_6}^*)\right] \tag{1.29}$$

Stability of the equilibrium points will depend on the sign of c and d, then the following stability analysis is made.

1. For $c > 0$ and $d > 0$: the eigenvalues is $Re[\lambda_{1,2} < 0]$, consequently the equilibrium points of the zero dynamics are stable. Working on the above inequalities, we find out a region related to $I_{L_6}^*$. The first region is given by $c > 0$:

$$\frac{V_{C_4} - \sqrt{\Delta_3}}{2R_{04}} < I_{L_6}^* < \frac{V_{C_4} + \sqrt{\Delta_3}}{2R_{04}} \tag{1.30}$$

where:

$$\Delta_3 = {V_{C_4}}^2 + 4R_{04} C_5 {V_{C_5}^e}^2 \left[\frac{1}{R_4 C_4} + \frac{1}{R_5 C_5}\right]$$

The second region given by $d > 0$ can be expressed as:

$$\frac{V_{C_4} - \sqrt{\Delta_4}}{2R_{04}} < I_{L_6}^* < \frac{V_{C_4} + \sqrt{\Delta_4}}{2R_{04}} \tag{1.31}$$

with:

$$\Delta_4 = {V_{C_4}}^2 + \frac{4R_{04}}{R_5}{V_{C_5}^e}^2$$

The intersection of (1.30) and (1.31) is actually given by (1.31), which is the region of stability for $I_{L_6}^*$.

2. For $c \geq 0$ and $d \leq 0$: at least one eigenvalue will have a positive real part $Re[\lambda_{1,2} \geq 0]$, then the system is not stable.

3. For $c \leq 0$: we also have at least one eigenvalue with positive real part $Re[\lambda_{1,2} \geq 0]$ where the zero dynamics are not stable.

The control of $I_{L_6} \rightarrow I_{L_6}^*$ is stable to charge and discharge the battery as long as the reference $I_{L_6}^*$ is designed respecting condition (1.31).

1.3.4 Feedback Linearization for PV Array

As said before, the PV array is designed to follow a reference given by the MPPT algorithm. Here we have considered the incremental conductance MPPT algorithm that is based on the calculation of the power derivative in the characteristic curve of the panel, and then the computation of the maximum of this function. The MPPT provides the reference value $I_{L_9}^*$ for the PV array such as to absorb the maximum solar power. According to the control objective, let us define the control output as $y_3 = I_{L_9}$. It is considered that the system has one output and one input. Thus, a square system is shown in (1.32).

$$\begin{cases} \dot{I}_{L_9} = f_3(V_{C_7}, V_{C_8}, I_{L_9}) + g_3 u_3 \\ y_3 = I_{L_9} \end{cases} \tag{1.32}$$

The Lie derivative of the output with respect to g_3 is:

$$J_3 = -\frac{V_{C_8} - (R_{08} - R_{07})I_{L_9}}{L_9}$$

J_3 is non-singular since $V_{C_8} \neq (R_{08} - R_{07})I_{L_9}$, therefore a nonlinear feedback control input can be written as:

$$\begin{aligned} u_3 &= J_3^{-1}\left[v_9 - \frac{1}{L_9}\left(V_{C_7} - V_{C_8} - R_{08}I_{L_9}\right)\right] \\ &= \frac{L_9 v_9 - V_{C_7} + V_{C_8} + R_{08}I_{L_9}}{V_{C_8} - (R_{08} - R_{07})I_{L_9}} \end{aligned}$$

where u_3 is the control input in (1.32) and v_9 is the additional input.

Since $I_{L_9}^*$ is the desired trajectory for I_{L_3}, it is possible to design the additional input v_9 in a linear manner with respect to the output I_{L_9} and hence a linear stable subspace is generated.

$$\begin{aligned} v_9 &= \dot{I}_{L_9}^* - K_9(I_{L_9} - I_{L_9}^*) - K_9^{\alpha}\alpha_9 \\ \dot{\alpha_9} &= I_{L_9} - I_{L_9}^* \end{aligned}$$

where K_9 and K_9^α are positive constants.

v_9 is the desired dynamics of I_{L_9} and α_9 is an auxiliary variable. This can be interpreted as a pole placement from linear control theory.

Zero dynamics

The states V_{C_7} and V_{C_8} are the zero dynamics in the PV system. The calculated equilibrium points are given by:

$$V_{C_7}^e = V_{PV} - R_7 I_{L_9}^*$$

$$V_{C_8}^e = \frac{V_{dc}}{2} \pm \frac{1}{2}\sqrt{V_{dc}^2 + 4R_7 I_{L_9}^*(V_{C_7} - R_{07} I_{L_9}^*)}$$

To analyze the zero dynamics stability, the Jacobian linearization matrix C is presented bellow:

$$C = \begin{bmatrix} -\frac{1}{R_7 C_7} & 0 \\ \frac{-I_{L_9}^*}{C_8[V_{C_8}^e - (R_{08}-R_{07})I_{L_9}^*]} & -\frac{1}{C_8 R_8} - \frac{I_{L_9}^*[V_{C_7} - (2R_{08}-R_{07})I_{L_9}^*]}{C_8[V_{C_8}^e - (R_{08}-R_{07})I_{L_9}^*]^2} \end{bmatrix}$$

In this case, we have that $I_{L_9} \geq 0$ is always positive, as a consequence $V_{PV} \geq V_{C_7}$. Therefore, we have only two possible cases in the matrix C parameters:

1. For $V_{C_7} - (2R_{08} - R_{07})I_{L_9}^* < 0$, we may result in:

$$V_{C_7}\frac{R_7 + (2R_{08} - R_{07})}{2R_{08} - R_{07}} < V_{PV} \tag{1.33}$$

   which is not physically possible, then this case is not considered.

2. For $V_{C_7} - (2R_{08} - R_{07})I_{L_9}^* > 0$, we may result in:

$$V_{C_7}\frac{R_7 + (2R_{08} - R_{07})}{2R_{08} - R_{07}} > V_{PV} \tag{1.34}$$

   In this case, the main diagonal terms of C is always positive, which result in negative eigenvalues related to linearization matrix C. Therefore, the zero dynamics is locally stable.

1.3.5 Feedback Linearization for DC load

The DC load must have a constant voltage supply, and then the reference value is defined as $V_{C_{11}}^*$. The output control $y_4 = V_{C_{11}}$, then the relative degree is 2. The DC load model can be represented as follows:

$$\begin{cases} \dot{V}_{C_{11}} = f_{11}(V_L, V_{C_{11}}) + g_{11} I_{L_{13}} \\ \dot{I}_{I_{13}} = f_{13}(V_{C_{11}}, V_{C_{12}}, V_{dc}) + g_{13}(V_{C_{12}}, I_{L_{13}})u_4 \\ y_4 = V_{C_{11}} \end{cases} \tag{1.35}$$

Using feedback linearization techniques, we take the derivative of the control output $V_{C_{11}}$ until obtaining the control input u_4. The following Lie derivatives can be deduced as:

$$\dot{V}_{C_{11}} = L^1_{f_{11}} h_{11}(x) \tag{1.36}$$

$$\begin{aligned} C_{11}\ddot{V}_{C_{11}} = &-\frac{1}{R_{11}}\left[\frac{1}{R_{11}C_{11}}(V_L - V_{C_{11}}) + \frac{1}{C_{11}} I_{L_{13}}\right] - \\ &+\frac{1}{L_{13}}\left[V_{C_{11}} + R_{011} I_{L_{13}} + [V_{C_{12}} - (R_{012} - R_{011}) I_{L_{13}}] u_4\right] \end{aligned} \tag{1.37}$$

$$\ddot{V}_{C_{11}} = L^2_{f_{11}} h_{11}(x) + L_{g_{11}} L^1_{f_{11}} h_{11}(x) u_4 \tag{1.38}$$

By introducing a synthetic input v_{11}, the input u_4 can be designed as:

$$u_4 = \frac{1}{L_{g_{11}} L^1_{f_{11}} h_{11}(x)} [v_{11} - L^2_{f_{11}} h_{11}(x)]$$

where the additional input is chosen using linear techniques to give the desired dynamics for $V_{C_{11}}$.

$$v_{11} = -K_{11}(\dot{V}_{C_{11}} - \dot{V}^*_{C_{11}}) - K^\alpha_{11}(V_{C_{11}} - V^*_{C_{11}})$$

where K_{11} and K^α_{11} are positive constants.

Zero dynamics

The state $V_{C_{12}}$ is the zero dynamics here, where the local stability analysis is given.

$$\dot{V}_{C_{12}} = \frac{1}{R_{12}C_{12}}(V_{dc} - V_{C_{12}}) - \frac{1}{C_{12}} I^*_{L_{13}} u^*_4 \tag{1.39}$$

where $I^*_{L_{13}} = \frac{1}{R_{11}}(V^*_{C_{11}} - V_L)$ and:

$$u^*_4 = \frac{V^*_{C_{11}} + R_{011} I^*_{L_{13}}}{V_{C_{12}} - (R_{012} - R_{011}) I^*_{L_{13}}}$$

To analyze the dynamics above, let us consider its linearization. The needed equilibrium points can be determined in (1.40).

$$V^e_{C_{12}} = -\frac{a_{12}}{2} \pm \frac{1}{2}\sqrt{a^2_{12} + 4\Delta_{12}} \tag{1.40}$$

where:

$$a_{12} = V_{dc} - (R_{012} - R_{011}) I^*_{L_{13}}$$

$$\Delta_{12} = I^*_{L_{13}}\left[(R_{012} - R_{011})V_{dc} + R_{12}(V_{C_{11}} + R_{011}I^*_{L_{13}})\right]$$

The linearization of the $V_{C_{12}}$ dynamical equation is obtained with the Jacobian equation in (1.41).

$$J_{12} = -\frac{1}{R_{12}C_{12}} + \frac{I^*_{L_{13}}}{C_{12}}\left\{\frac{V^*_{C_{11}} + R_{011}I^*_{L_{13}}}{[V^e_{C_{12}} - (R_{012} - R_{011})I^*_{L_{13}}]^2}\right\} \tag{1.41}$$

In the DC load case, we have that $I^*_{L_{13}} \geq 0$, as a consequence we can also state that $V_L < V_{C_{11}}$. Let us now take into account all possible cases:

1. For $V^*_{C_{11}} + R_{011}I^*_{L_{13}} > 0$, we may result in:

$$V^*_{C_{11}}\frac{R_{11} + R_{011}}{R_{011}} > V_L \tag{1.42}$$

   which is not physically possible, then this case is not considered.

2. For $V^*_{C_{11}} + R_{011}I^*_{L_{13}} < 0$, we may result in:

$$V^*_{C_{11}}\frac{R_{11} + R_{011}}{R_{011}} < V_L \tag{1.43}$$

   which is a possible case that results in always negative value for Jacobian linearization J_{12}. Therefore the zero dynamics is locally stable.

1.4 Simulations

Simulink's toolbox *SimPowerSystem* allows to model a realist power system including power electronics devices like IGBT, MOSFET, and GTO, sources, loads, and basic elements like resistances, capacitors, and inductors providing a powerful simulation environment. Besides that, control algorithms can be easily developed on Simulink environment, which makes Simulink environment the standard platform for simulation of complex systems like MicroGrids.

The DC MicroGrid was built using *SimPowerSystem* toolbox from Matlab/Simulink, with a realistic model and the proposed control laws. The simulations are focused on showing the transient behavior of the system and the proposed nonlinear control performance. The time range for simulations is 15 s during which the supercapacitor works to keep the stability of the DC bus. Table 1.1 presents the parameters of the MicroGrid. In this simulation example, the DC bus is modeled as capacitor with a small capacitance of $C_{10} = 100\ \mu F$ (representing fast voltage dynamics) and the desired voltage on DC bus is $V^*_{dc} = 630\ V$. The supercapacitor is composed of 18 series capacitors and 4 parallel capacitors forming a capacitance of 100 F with 420 V of rated voltage, and the equivalent DC series resistance is 9 Ω. The battery is an ion-lithium one with 380 kWh of energy capacity and 160 kW of power capacity with nominal voltage of 380 V. The PV system is composed of 15 modules in series and 100 modules in parallel

Table 1.1: MicroGrid parameters

Supercap	**Battery**	**PV**	**Load**	**Value**
R_1	R_4	R_7	R_{11}	0.1 Ω
C_1	C_4	C_7	C_{11}	10 mF
R_2	R_5	R_8	R_{12}	0.1 Ω
C_2	C_5	C_8	C_{12}	10 mF
L_3	L_6	L_9	L_{13}	3.3 mH
R_{01}	R_{04}	R_{07}	R_{011}	10 $m\Omega$
R_{02}	R_{05}	R_{08}	R_{012}	10 $m\Omega$

of 60 W resulting in 90 kW of nominal power. The DC load is a time-varying one with 50 kW of maximum consumption.

Figure 1.4 presents the incident irradiation in the PV and the current demand in the DC load respectively. The irradiation causes large excursion in the power generation from the PV, in the same way as the demanded current varies following the power needs from the load, and therefore both parameters bring strong time-varying disturbances to the MicroGrid.

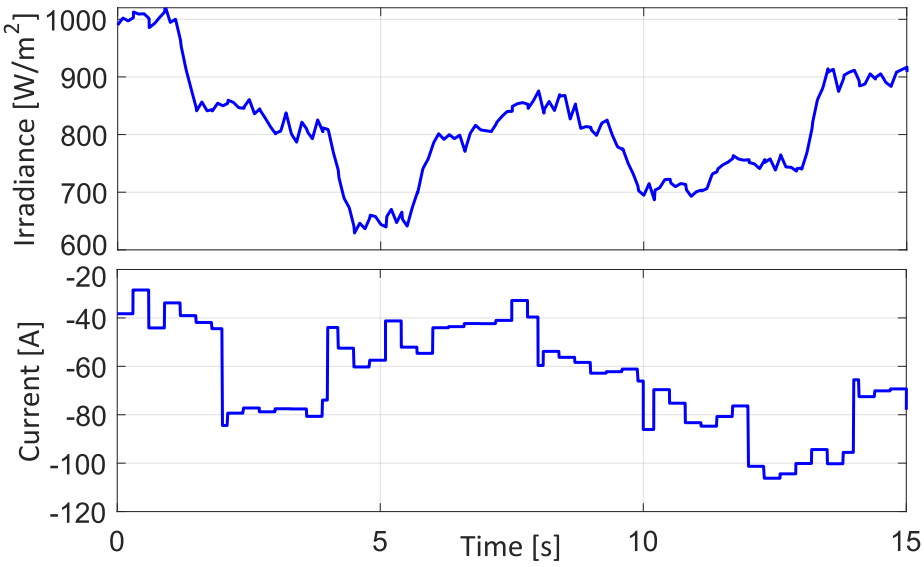

Figure 1.4: The incident irradiation on PV and the demanded current on DC load,respectivaly.

Figure 1.5 presents the voltage on supercapacitor, battery, and PV array, respectively. The supercapacitor voltage varies according to the absorption/injection of power into the grid. The same behavior in the battery voltage can be observed. The PV voltage varies according to the irradiation profile in Figure 1.4.

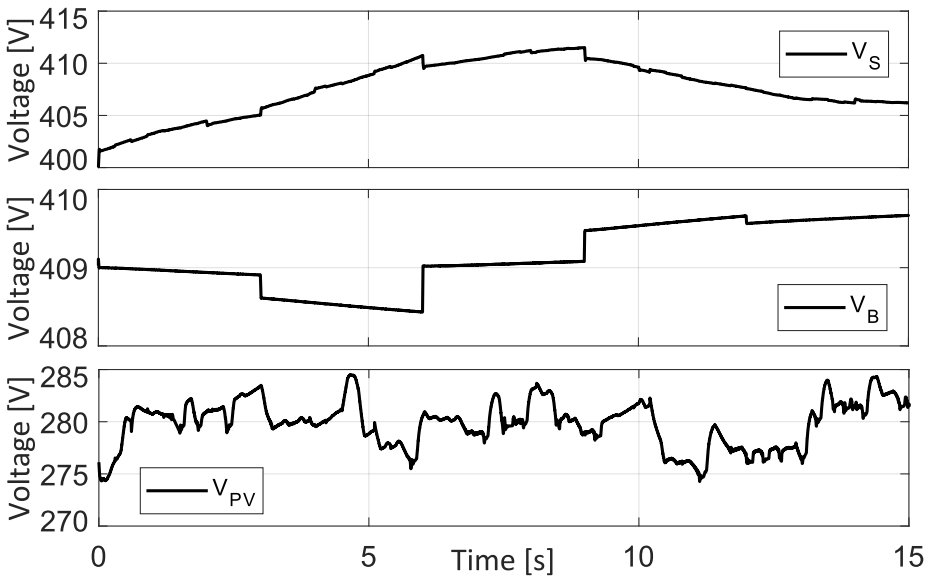

Figure 1.5: Voltage on supercapacitor V_S, battery V_B and PV array V_{PV}, respectively.

Figure 1.6 presents the controlled voltage on DC load $V_{C_{11}}$ and its reference. The voltage is controlled with fast control response, and the highest peaks represents variations about 0.6%, which is inside of the grid requirements. In conclusion, the MicroGrid control accomplish the target to feed the DC load correctly.

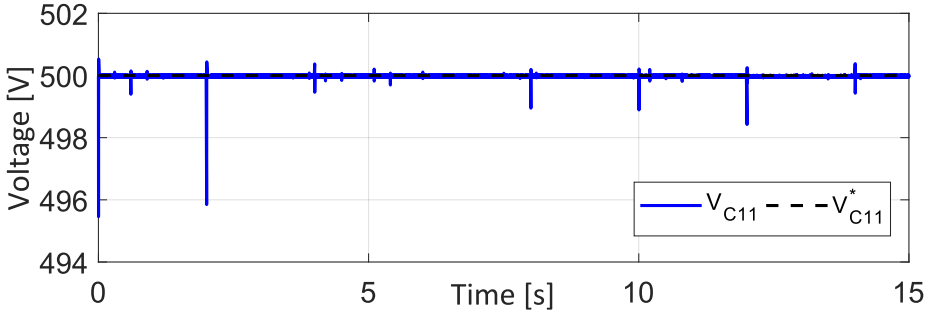

Figure 1.6: The controlled voltage on the DC load and its reference.

Figure 1.7 presents the controlled currents on supercapacitor I_{L_3}, battery I_{L_6} and their references. Current I_{L_3} is given by the current demand in the DC load, the current flowing from the battery and the current generated in the PV system. Current I_{L_6} has much slower variations following the second level controller reference. The currents track their reference with good performance.

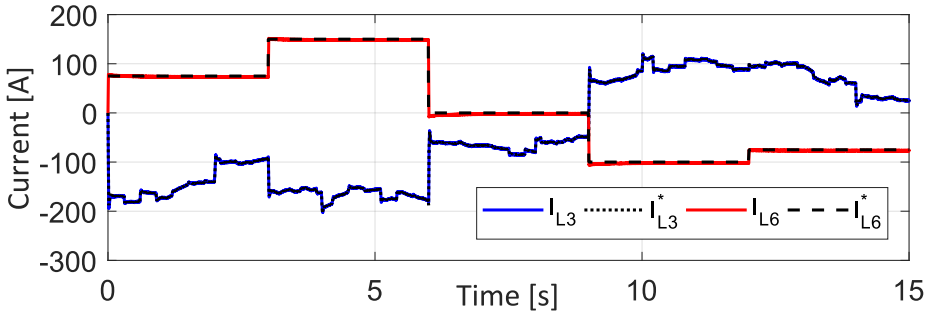

Figure 1.7: The current on the supercapacitor I_{L_3} in blue and the current in the battery I_{L_6} in red.

Figure 1.8 presents controlled current I_{L_9} on the PV system and its reference given by the MPPT algorithm. As the irradiation profile also influences the current, its variations are quite similar to each other.

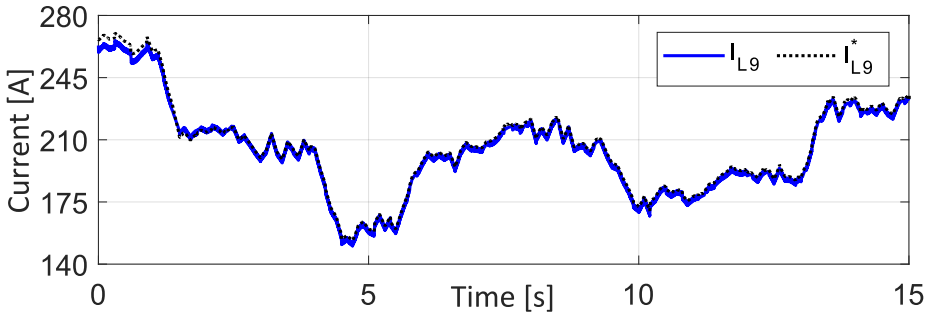

Figure 1.8: The controlled current on PV and its reference given by MPPT algorithm.

Figure 1.9 presents the current demand in the DC load $I_{L_{13}}$ and its reference $I^*_{L_{13}}$. The current follows its reference varying in order to guarantee the power supply for the DC load, allowing good control performance, such that voltage is also well controlled.

Figure 1.10 presents the output voltages from the converters that connect the devices (battery, PV and DC load) into the MicroGrid by the DC bus. they represent the zero dynamics of proposed control target, it is concluded that the variables present stable behavior.

Voltage V_{C_2} and calculated reference $V^*_{C_2}$ are depicted in Figure 1.11. The reference $V^*_{C_2}$ is calculated to provide the regulation of the voltage in the DC bus; then the supercapacitor is allowed to stabilize the voltage in the MicroGrid by injecting or absorbing the mistaken power to balance the grid.

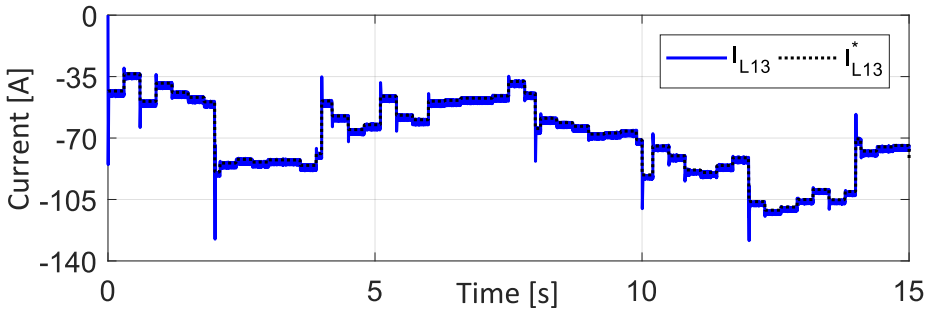

Figure 1.9: The current demanded by the DC load.

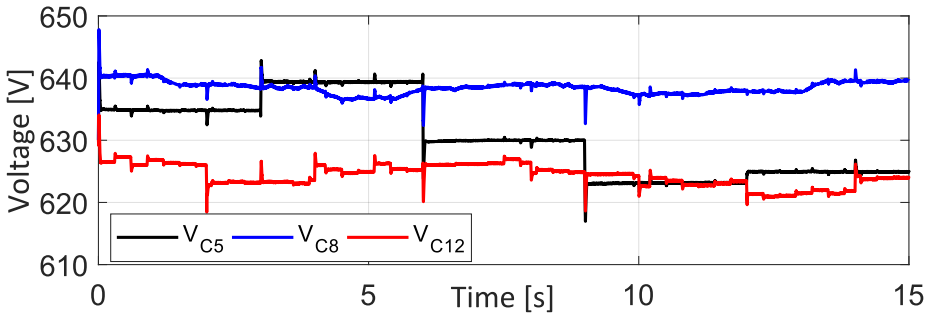

Figure 1.10: Output voltages on the MicroGrid converters (zero dynamics).

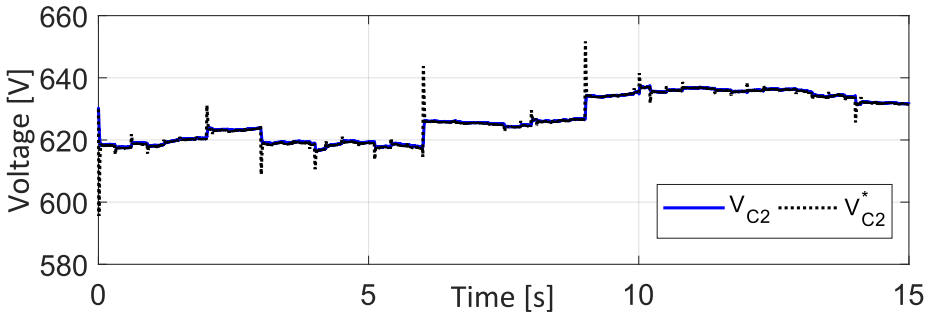

Figure 1.11: Voltage V_{C_2} and its reference.

The DC bus voltage Vdc is presented in Figure1.12. The voltage is controlled in the desired value V_{dc}, and the transient error is 1.3% maximum. In conclusion, the voltage V_{dc} meets the grid requirements with good control performance. The good behavior of V_{dc} allows proper operation in the MicroGrid, where the power balance is obtained.

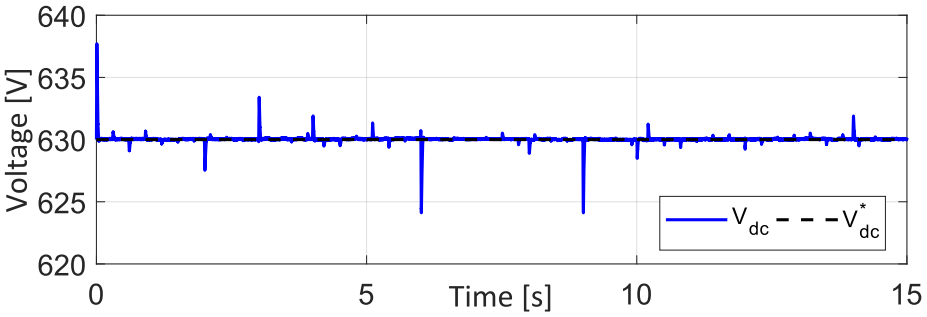

Figure 1.12: DC voltage bus and the operation bounds.

1.4.1 A control comparison: Linear vs Nonlinear

The PI controller is widely known and disseminated both in academia and in the industry for its simplicity of application and robustness. However, in the case of electrical systems that require better performance and greater energy efficiency, nonlinear control approach becomes a better option. To verify this idea, a comparison of the proposed nonlinear control with the classic linear control approach was carried out in the considered MicroGrid.

Figure 1.13 compares the different voltage behaviors in the DC bus, using a nonlinear controller (in red) and classical PI controller (in blue). The dynamic behavior of the nonlinear approach ishas faster convergence rate with smaller overshoots in the transients, besides that, the nonlinear dynamics is smoother than the linear one. Also, since the nonlinear control considers the different nonlinearities, it has a larger operating region and there is no need to tune the gains continuously according to the different operating point. In extensive set of simulations carried out exploring the effects of several disturbances, it was necessary to re-adjust the PI parameters for each case. While in the same simulations the nonlinear control has always kept the same tunning. In the same way, the nonlinear tunning is a trivial pole placement problem for all elements, while for the PI it is necessary to use one of the standard methods like root locus, but with complex interferences between one controller setting to the others. In conclusion, the nonlinear control approach can stabilize the DC bus from the MicroGrid with better performance, which illustrates the limitations of the linear control for a wide region of operation.

1.5 Concluding Remarks

In this chapter, the concept of DC MicroGrids is introduced. Renewable energy sources, energy storage systems, and loads are the basics components of a DC MicroGrid. The DC nature of these devices greatly simplifies their integration in DC MicroGrids, thus making power converter topology and the control structure simpler. It is crucial for proper operation of the system a hierarchical

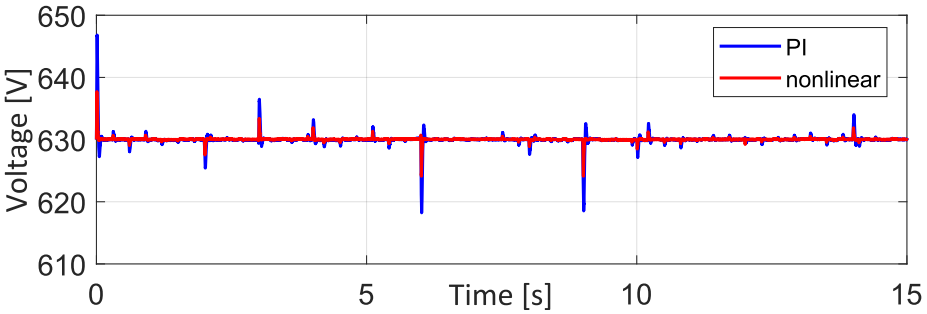

Figure 1.13: DC bus voltage dynamics comparing the proposed nonlinear control and the linear PI controller.

control structure that accomplishes the MicroGrid targets from transients in milliseconds to energy dispatch in hours. The MicroGrid modeling based on the average model of power converters is developed to establish the dynamics of the system. A nonlinear control strategy was designed based on control-induced time-scale separation, where the controllers induce a singular perturbation behavior that is not natural to the system. This approach allows to develop a much simpler controller at the expense of an explicit operation region, and with the realization that some small dynamics are neglected. Lyapunov theory provides the stability analysis for the whole system, where the DC bus is controlled to maintain the operation of the MicroGrid devices. The proposed controller shows very good behavior, and even when compared with the industry's standard PI it allows for a better performance.

Bibliography

[1] E. Planas, A. Gil-de Muro, J. Andreu, I. Kortabarria, and I. M. de Alegría, "General aspects, hierarchical controls and droop methods in microgrids: A review," *Renewable and Sustainable Energy Reviews*, vol. 17, pp. 147–159, 2013.

[2] P. M. Costa and M. A. Matos, "Economic analysis of microgrids including reliability aspects," in *2006 International Conference on Probabilistic Methods Applied to Power Systems*, June 2006, pp. 1–8.

[3] L. E. Zubieta, "Are microgrids the future of energy?: Dc microgrids from concept to demonstration to deployment," *IEEE Electrification Magazine*, vol. 4, no. 2, pp. 37–44, June 2016.

[4] T. Dragicevic, J. C. Vasquez, J. M. Guerrero, and D. Skrlec, "Advanced lvdc electrical power architectures and microgrids: A step toward a new generation of power distribution networks." *IEEE Electrification Magazine*, vol. 2, no. 1, pp. 54–65, March 2014.

[5] D. E. Olivares, A. Mehrizi-Sani, A. H. Etemadi, C. A. Cañizares, R. Iravani, M. Kazerani, A. H. Hajimiragha, O. Gomis-Bellmunt, M. Saeedifard, R. Palma-Behnke, G. A. Jiménez-Estévez, and N. D. Hatziargyriou, "Trends in microgrid control," *IEEE Transactions on Smart Grid*, vol. 5, no. 4, pp. 1905–1919, July 2014.

[6] W. Jing, C. H. Lai, S. H. W. Wong, and M. L. D. Wong, "Battery-supercapacitor hybrid energy storage system in standalone dc microgrids: areview," *IET Renewable Power Generation*, vol. 11, no. 4, pp. 461–469, 2017.

[7] J. J. Justo, F. Mwasilu, J. Lee, and J.-W. Jung, "Ac-microgrids versus dc-microgrids with distributed energy resources: A review," *Renewable and Sustainable Energy Reviews*, vol. 24, pp. 387–405, 2013.

[8] E. Unamuno and J. A. Barrena, "Hybrid ac/dc microgrids—part ii: Review and classification of control strategies," *Renewable and Sustainable Energy Reviews*, vol. 52, pp. 1123–1134, 2015.

[9] A. A. Akhil, G. Huff, A. B. Currier, B. C. Kaun, D. M. Rastler, S. B. Chen, A. L. Cotter, D. T. Bradshaw, and W. D. Gauntlett, *DOE/EPRI 2013 electricity storage handbook in collaboration with NRECA*. Sandia National Laboratories Albuquerque, NM, 2013.

[10] F. Locment, M. Sechilariu, and I. Houssamo, "Dc load and batteries control limitations for photovoltaic systems. experimental validation," *IEEE Transactions on Power Electronics*, vol. 27, no. 9, pp. 4030–4038, Sept 2012.

[11] P. F. Ribeiro, B. K. Johnson, M. L. Crow, A. Arsoy, and Y. Liu, "Energy storage systems for advanced power applications," *Proceedings of the IEEE*, vol. 89, no. 12, pp. 1744–1756, 2001.

[12] J. G. de Matos, F. S. F. e Silva, and L. A. d. S. Ribeiro, "Power control in ac isolated microgrids with renewable energy sources and energy storage systems," *IEEE Transactions on Industrial Electronics*, vol. 62, no. 6, pp. 3490–3498, June 2015.

[13] L. A. de Souza Ribeiro, O. R. Saavedra, S. L. de Lima, and J. G. de Matos, "Isolated micro-grids with renewable hybrid generation: The case of lençóis island,"," *IEEE Transactions on Sustainable Energy*, vol. 2, no. 1, pp. 1–11, Jan 2011.

[14] L. A. d. S. Ribeiro, O. R. Saavedra, S. L. Lima, J. G. de Matos, and G. Bonan, "Making isolated renewable energy systems more reliable," *Renewable Energy*, vol. 45, pp. 221–231, 2012.

[15] R. H. Lasseter, "Smart distribution: Coupled microgrids," *Proceedings of the IEEE*, vol. 99, no. 6, pp. 1074–1082, 2011.

[16] D. Kumar, F. Zare, and A. Ghosh, "Dc microgrid technology: System architectures, ac grid interfaces, grounding schemes, power quality, communication networks, applications, and standardizations aspects," *Ieee Access*, vol. 5, pp. 12 230–12 256, 2017.

[17] T. Dragičević, X. Lu, J. C. Vasquez, and J. M. Guerrero, "Dc microgrids—part i: A review of control strategies and stabilization techniques," *IEEE Transactions on power electronics*, vol. 31, no. 7, pp. 4876–4891, 2016.

[18] N. Yang, B. Nahid-Mobarakeh, F. Gao, D. Paire, A. Miraoui, and W. Liu, "Modeling and stability analysis of multi-time scale dc microgrid," *Electric Power Systems Research*, vol. 140, pp. 906–916, 2016.

[19] S. M. Ashabani and Y. A. r. I. Mohamed, "New family of microgrid control and management strategies in smart distribution grids; analysis, comparison and testing," *IEEE Transactions on Power Systems*, vol. 29, no. 5, pp. 2257–2269, Sept 2014.

[20] E. Rokrok, M. Shafie-Khah, and J. P. S. Catalão, "Comparison of two control strategies in an autonomous hybrid microgrid," in *2017 IEEE PES Innovative Smart Grid Technologies Conference Europe (ISGT-Europe)*, Sept 2017, pp. 1–6.

[21] A. Iovine, S. B. Siad, G. Damm, E. D. Santis, and M. D. D. Benedetto, "Nonlinear control of a dc microgrid for the integration of photovoltaic panels," *IEEE Transactions on Automation Science and Engineering*, vol. 14, no. 2, pp. 524–535, April 2017.

[22] ——, "Nonlinear control of an ac-connected dc microgrid," in *IECON 2016 - 42nd Annual Conference of the IEEE Industrial Electronics Society*, Oct 2016, pp. 4193–4198.

[23] A. P. N. Tahim, D. J. Pagano, and E. Ponce, "Nonlinear control of dc-dc bidirectional converters in stand-alone dc microgrids," in *2012 IEEE 51st IEEE Conference on Decision and Control (CDC)*, Dec 2012, pp. 3068–3073.

[24] C. Wang, X. Li, L. Guo, and Y. W. Li, "A nonlinear-disturbance-observer-based dc-bus voltage control for a hybrid ac/dc microgrid," *IEEE Transactions on Power Electronics*, vol. 29, no. 11, pp. 6162–6177, Nov 2014.

[25] S. Parhizi, H. Lotfi, A. Khodaei, and S. Bahramirad, "State of the art in research on microgrids: A review," *Ieee Access*, vol. 3, pp. 890–925, 2015.

[26] T. Morstyn, B. Hredzak, and V. G. Agelidis, "Control strategies for microgrids with distributed energy storage systems: An overview," *IEEE Transactions on Smart Grid*, vol. 9, no. 4, pp. 3652–3666, July 2018.

[27] J. M. Guerrero, J. C. Vasquez, J. Matas, L. G. De Vicuña, and M. Castilla, "Hierarchical control of droop-controlled ac and dc microgrids—a general approach toward standardization," *IEEE Transactions on industrial electronics*, vol. 58, no. 1, pp. 158–172, 2011.

[28] A. Iovine, "Nonlinear and hybrid control techniques for microgrids and autonomous vehicles," Ph.D. dissertation, L'Aquila University, 2016.

[29] A. Bidram and A. Davoudi, "Hierarchical structure of microgrids control system," *IEEE Transactions on Smart Grid*, vol. 3, no. 4, pp. 1963–1976, 2012.

[30] F. A. Inthamoussou, J. Pegueroles-Queralt, and F. D. Bianchi, "Control of a supercapacitor energy storage system for microgrid applications," *IEEE Transactions on Energy Conversion*, vol. 28, no. 3, pp. 690–697, Sept 2013.

[31] V. A. Boicea, "Energy storage technologies: The past and the present," *Proceedings of the IEEE*, vol. 102, no. 11, pp. 1777–1794, Nov 2014.

[32] D. Sera, L. Mathe, T. Kerekes, S. V. Spataru, and R. Teodorescu, "On the perturb-and-observe and incremental conductance mppt methods for pv systems," *IEEE Journal of Photovoltaics*, vol. 3, no. 3, pp. 1070–1078, July 2013.

[33] D. C. Huynh and M. W. Dunnigan, "Development and comparison of an improved incremental conductance algorithm for tracking the mpp of a solar pv panel," *IEEE Transactions on Sustainable Energy*, vol. 7, no. 4, pp. 1421–1429, Oct 2016.

[34] Y. Chen, "Nonlinear control and stability analysis of multi-terminal high voltage direct current networks," Ph.D. dissertation, Université Paris-Sud, 2015.

[35] Y. Chen, G. Damm, A. Benchaib, and F. Lamnabhi-Lagarrigue, "Feedback linearization for the dc voltage control of a vsc-hvdc terminal," in *2014 European Control Conference (ECC)*, June 2014, pp. 1999–2004.

[36] P. Rouchon, "Necessary condition and genericity of dynamic feedback linearization," *J. Math. Systems Estim. Control*, vol. 4, no. 2, pp. 257–260, 1994.

[37] B. Charlet, J. Lévine, and R. Marino, "On dynamic feedback linearization," *Systems & Control Letters*, vol. 13, no. 2, pp. 143–151, 1989.

[38] G. Oriolo, A. D. Luca, and M. Vendittelli, "Wmr control via dynamic feedback linearization: design, implementation, and experimental validation," *IEEE Transactions on Control Systems Technology*, vol. 10, no. 6, pp. 835–852, Nov 2002.

[39] R. Marino, "Static and dynamic feedback linearization of nonlinear systems," in *Perspectives in control theory*. Springer, 1990, pp. 249–260.

[40] A. Iovine, S. Damm, E. D. Santis, M. D. D. Benedetto, L. Galai-Dol, and P. Pepe, "Voltage stabilization in a dc microgrid by an iss-like lyapunov function implementing droop control," in *ECC 2018 - European Control Conference*, Jun 2018, pp. 4193–4198.

[41] E. D. Sontag, "Input to state stability: Basic concepts and results," in *Nonlinear and optimal control theory*. Springer, 2008, pp. 163–220.

[42] H. K. Khalil, *Nonlinear control*. Prentice Hall, 2014.